essary condition for gelation even in the case of such a highly crystalline polymer.

There are five pieces of evidence showing that the gelation is caused by liquid–liquid phase separation:

(1) Gelation occurred in a transparent state (section 1.3 and Figure 12).

(2) Some semitransparent gels existed in an equilibrium state between transparent and opaque gel (Figure 12). This shows that crystallization proceeds in the polymer-rich phase.

(3) Two types of crystal forms appeared in one gel when some of the semitransparent gels were cooled to completely crystallize (two-step crystallization) (Figure 13a). The crystal form was different in the polymer-rich and polymer-poor phases.

(4) Some of the two-step crystallized gels showed two-step dissolution on heating (Figure 14). With increasing temperature, the crystallites in the polymer-poor phase dissolved at a lower temperature and then those in the polymer-rich phase dissolved.

(5) The optical morphology of the dried gels left a trace that is characteristic for liquid–liquid phase separation (Figures 6a and 13b). This is indirect evidence of the existence of the two phases that had formed at the early stage of gelation without crystallization.

From the above discussion, the boundary line between regions A and B means the binodal curve. Regelation extends the gel region to higher temperatures (Figures 10 and 11). Why can the gelation region be easily enlarged by regelation? It would be more reasonable that the particular molecular interaction formed between the solvent and polymer at 0 °C could live on even after melting at 90 °C and become the trigger that easily induces the liquid–liquid phase separation at the subsequent regelation stage. The interaction may be related to the freezing of the solvent because 0 °C is lower than the freezing point of the pure solvent.

We observed two kinds of gel structure. The structure for the liquid–liquid phase separation is very similar to that of Keller's model as regards the duplicity of the structure. The aggregated structure for the solid–liquid phase separation has not yet been found in the gels of poorly crystallizable polymers such as iPS and PVC. In the latter polymers the fringed micelle crystallite may be more acceptable rather than the lamella-like one. However, we could not observe in our gels positive evidence for the existence of the fringed micelle. If a phase diagram like that in Figure 2 was drawn also for the iPS system, more strict comparison would be made between the two polymers.

Acknowledgment. We thank Dr. Keizo Miyasaka for inviting us to study P4M1P. We are also grateful to Dr. Hiroshi Ishikawa and Dr. Masanobu Nagura for the use of X-ray diffraction apparatus.

Registry No. Isotactic P4M1P, 24979-98-4; cyclohexane, 110-82-7.

References and Notes

(1) Wellinghoff, S. W.; Shaw, J.; Baer, E. *Macromolecules* **1979**, *12*, 932.
(2) Tan, M. H.; Moet, A.; Hiltner, A.; Baer, E. *Macromolecules* **1983**, *16*, 28.
(3) Ogasawara, K.; Nakajima, T.; Yamaura, K.; Matsuzawa, S. *Prog. Colloid Polym. Sci.* **1975**, *58*, 145.
(4) Ogasawara, K.; Nakajima, T.; Yamaura, K.; Matsuzawa, S. *Colloid Polym. Sci.* **1976**, *254*, 456.
(5) Ogasawara, K.; Nakajima, T.; Yamaura, K.; Matsuzawa, S. *Colloid Polym. Sci.* **1976**, *254*, 553.
(6) Ogasawara, K.; Nakajima, T.; Yamaura, K.; Matsuzawa, S. *Colloid Polym. Sci.* **1976**, *254*, 982.
(7) Matsuzawa, S.; Yamaura, K.; Maeda, R.; Ogasawara, K. *Makromol. Chem.* **1979**, *180*, 229.
(8) Girolamo, M.; Keller, A.; Miyasaka, K.; Overbergh, N. *J. Polym. Sci., Polym. Phys. Ed.* **1976**, *14*, 39.
(9) Atkins, E. D. T.; Isaac, D. H.; Keller, A.; Miyasaka, K. *J. Polym. Sci., Polym. Phys. Ed.* **1977**, *15*, 211.
(10) Atkins, E. D. T.; Isaac, D. H.; Keller, A. *J. Polym. Sci., Polym. Phys. Ed.* **1980**, *18*, 71.
(11) Atkins, E. D. T.; Keller, A.; Shapiro, J. S.; Lemstra, P. J. *Polymer* **1981**, *22*, 1161.
(12) Lemstra, P. J.; Keller, A.; Cudby, M. *J. Polym. Sci., Polym. Phys. Ed.* **1978**, *16*, 1507.
(13) Guerrero, S. J.; Keller, A.; Soni, P. L.; Geil, P. H. *J. Polym. Sci., Polym. Phys. Ed.* **1980**, *18*, 1533.
(14) Guerrero, S. J.; Keller, A.; Soni, P. L.; Geil, P. H. *J. Macromol. Sci., Phys.* **1981**, *B20*, 161.
(15) Guerrero, S. J.; Keller, A. *J. Macromol. Sci., Phys.* **1981**, *B20*, 167.
(16) Aharoni, S. M.; Charlet, G.; Delmas, G. *Macromolecules* **1981**, *14*, 1390.
(17) Charlet, G.; Delmas, G. *Polym. Bull. (Berlin)* **1982**, *6*, 367.
(18) Eldridge, J. E.; Ferry, J. D. *J. Phys. Chem.* **1954**, *58*, 992.
(19) Tanda, Y.; Imada, K.; Takayanagi, M. *Kogyo Kagaku Zasshi* **1966**, *69*, 1971.
(20) Takayanagi, M.; Kawasaki, N. *J. Macromol. Sci., Phys.* **1967**, *B1*, 741.

Polarized Raman Spectra and LO–TO Splitting of Poly(vinylidene fluoride) Crystal Form I

Kohji Tashiro,* Yuzo Itoh, Masamichi Kobayashi, and Hiroyuki Tadokoro

Department of Macromolecular Science, Faculty of Science, Osaka University, Toyonaka, Osaka 560, Japan. *Received May 2, 1985*

ABSTRACT: An LO–TO splitting ($\Delta\omega = \omega_{LO} - \omega_{TO}$) of Raman bands has been observed for poling-treated poly(vinylidene fluoride) (PVDF) crystal form I, where ω_{LO} and ω_{TO} are vibrational frequencies of longitudinal and transverse optical modes, respectively. The measured $\Delta\omega$ was about 1–6 cm^{-1}. The lattice dynamically predicted relationship, $A \propto \omega_{TO}\Delta\omega$ (A = infrared absorbance), has been confirmed experimentally. The band assignments for PVDF form I reported in the previous paper (Kobayashi, M.; Tashiro, K.; Tadokoro, H. *Macromolecules* **1975**, *8*, 158) have been revised on the basis of the polarization character of the infrared and Raman spectra and by carrying out the normal coordinate treatment.

Recently poly(vinylidene fluoride) (PVDF) crystal form I has been proved experimentally to be a ferroelectric material.[1,2] In such ferroelectric substances, in general, the long-range dipole–dipole interaction plays a very important role in their physical properties and ferroelectric phase transition behavior.[3] However, it may be difficult to es-

0024-9297/85/2218-2600$01.50/0

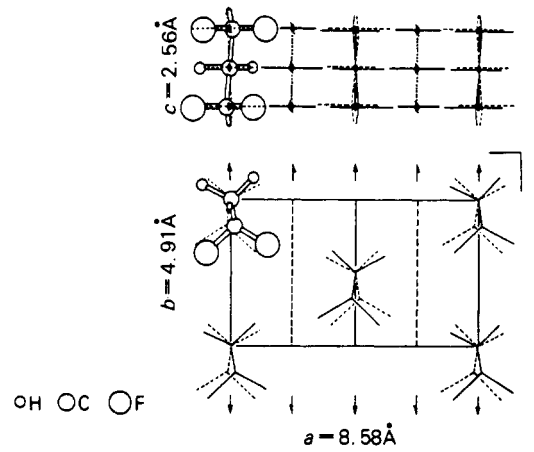

Figure 1. Crystal structure of PVDF form I.[11]

timate this dipole–dipole interaction quantitatively. One possible and useful method for this purpose is the measurement of the LO–TO splitting of polar phonons in the Raman spectra,[4-6] where LO and TO denote the longitudinal and transverse optical modes, respectively. When the charged atoms vibrate in the crystal lattice, a transition dipole moment $\boldsymbol{M}$ is generated for those vibrational modes that are active in infrared absorption. The phonon accompanying such a dipole change is called a "polar phonon". These dipoles generate a macroscopic electric field that couples in feedback fashion with the LO modes of the polar phonon, the transition moment $\boldsymbol{M}$ of which is along the propagation direction of the phonon $\boldsymbol{q}$ ($\boldsymbol{M} \parallel \boldsymbol{q}$). Due to the effect of these self-generated electrostatic forces, the vibrational frequency of the LO mode is shifted toward higher frequencies than that of the TO mode ($\boldsymbol{M} \perp \boldsymbol{q}$), the frequency of which is determined by the short-range interaction in the crystal lattice. This phenomenon is called an "LO–TO splitting" and is expected to be observed in the Raman spectra of the "infrared-active" polar phonons. In other words, when we measure the Raman spectra with changing the angle between the transition moment vector $\boldsymbol{M}$ and the phonon vector $\boldsymbol{q}$, we may expect some frequency shift for the Raman bands of the infrared-active polar vibrations.

The LO–TO splitting should be observed in principle for all crystals with noncentrosymmetric structures, but the magnitude of the frequency shift depends largely on the extent of the contribution of long-range electrostatic interactions. Therefore, the observation of the LO–TO splitting has been actually limited almost entirely to low-molecular-weight ionic crystals.[5] Only a few reports have been presented for molecular crystals such as trioxane,[7,8] pentaerythritol,[9] triglycine sulfate,[10] and others. As stated above, a rather large electrostatic field effect is expected for ferroelectric PVDF form I crystal. We have measured precisely the polarized Raman spectra of PVDF form I and succeeded in observing the LO–TO splitting. This is considered to be the first case for organic polymer materials. In this paper we report the Raman spectral change caused by poling treatment of PVDF form I and we then report the LO–TO splitting for this poled PVDF sample.

Group Theoretical Consideration

PVDF form I has the crystal structure shown in Figure 1, where the trans-zigzag chains are packed so that the CF_2 dipoles are parallel along the b axis.[11] The space group is $Cm2m$—C_{2v}^{14}. The result of a factor group analysis for the optically active Γ modes is shown in Table I. Among the four symmetry species, the A_1, B_1, and B_2 modes are infrared-active and the transition dipole moments are along the b, c, and a axes, respectively. The A_2 modes are nonpolar with no transition moment and are Raman active only. The polarizability tensor components are (aa), (bb), and (cc) for the A_1 modes, (ac) for the A_2 modes, (bc) for the B_1 modes, and (ab) for the B_2 modes. The tentative band assignments for PVDF form I have already been published in our previous paper.[12]

Table I
Factor Group Analysis for the Γ Modes of PVDF Form I Crystal (Space Group $Cm2m$—C_{2v}^{14})

symmetry species	E	C_2	σ_{ab}	σ_{bc}	μ'^a	α'^b	internal modes	external modes[c]
A_1	1	1	1	1	b	(aa), (bb), (cc)	5	T_b
A_2	1	1	−1	−1		(ac)	2	
B_1	1	−1	−1	1	c	(bc)	3	T_c
B_2	1	−1	1	−1	a	(ab)	4	T_a, L_c

[a] Transition dipole moment. [b] Raman polarizability tensor. [c] T, translational lattice mode; L, librational lattice mode.

Experimental Section

The PVDF sample used here was supplied by Kureha Chemical Co., Ltd. (KF 1000). After being quenched in an ice-water bath from the molten state, the sample was rolled at 80 °C with draw-ratio of about 500% and then annealed at ca. 130 °C for 1 h under tension. The film thickness was about 40 μm. The films were subjected to poling treatment under various conditions of high dc voltage (5–10 kV) and temperature (30–80 °C). The polarized infrared absorption spectra were measured with a Japan Spectroscopic Co. (JASCO) A-III type infrared spectrophotometer equipped with a wire-grid polarizer. The polarized Raman spectra were taken with JASCO R-500 and R-800 Raman spectrophotometers. The excitation light source was an Ar^+ ion laser with 514.5 nm wavelength.

Poling Effect on Polarized Infrared and Raman Spectra

In Figure 2 are reproduced the polarized infrared spectra of PVDF form I in the frequency region of 3200–400 cm^{-1}. As already pointed out by several authors,[13-16] when the PVDF film is poled under a high dc voltage, the dipole moment of the zigzag chain or the polar b axis is reoriented in the direction of the applied electric field. This situation is illustrated in Figure 3. In Figure 4 is shown the definition of the x, y, and z coordinate axes fixed on the film sample. Since the infrared absorption intensity is proportional to the scalar product of the transition dipole moment and the electric field vector of the incident infrared beam, we can expect that when the infrared beam is incident along the y axis with the electric vector $\boldsymbol{E}$ parallel to the x axis, the A_1 bands (the transition vector $\mu_b' \perp \boldsymbol{E}$) will decrease in intensity and the B_2 bands ($\mu_a' \parallel \boldsymbol{E}$) will increse in intensity after poling treatment.[15,16] The B_1 bands, which have the transition dipole μ_c' and are observed for the parallel polarization (E_z) of incident infrared beam, will show almost no change in their intensity even after poling. In Figure 2, we can see the decrease in intensity for the A_1 bands at 2980, 1273, and 840 cm^{-1}, and the increase for the B_2 bands at 3022 and 442 cm^{-1} by comparing the spectra taken before and after poling.

Figure 5 shows the polarized Raman spectra of rolled PVDF form I film before being subjected to the poling treatment. The B_1 bands at 1078 and 410 cm^{-1} appear relatively strongly for the (xz) polarization and the A_2 bands at 980 and 260 cm^{-1} appear for the (yz) polarization. According to the above group theoretical consideration, the B_1 bands should be observed strongly for the (bc) polarization component and those of the A_2 symmetry species should be observed for the (ac) polarization component. In Figure 5, such a situation can be realized if the

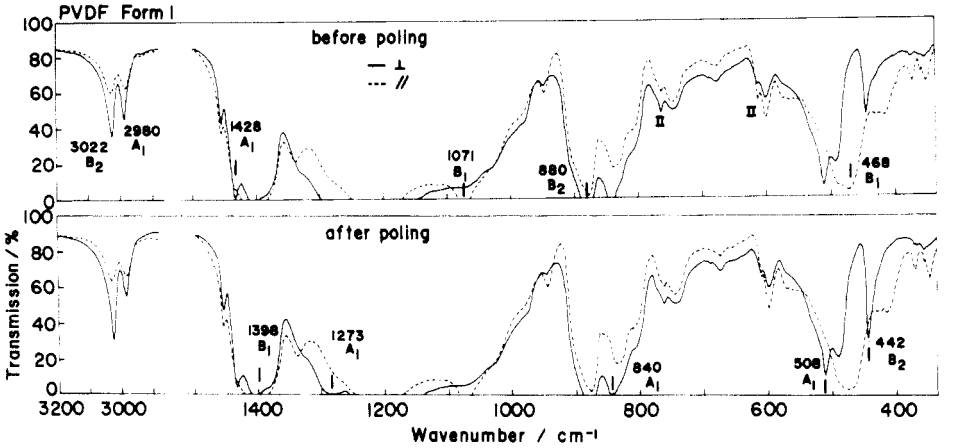

Figure 2. Polarized infrared spectra of PVDF form I taken before and after poling (conventional poling, E_p = 125 MV/m, 80 °C, 1 h): (—) electric vector of incident infrared beam perpendicular to the draw axis; (---) electric vector of incident infrared beam parallel to the draw axis.

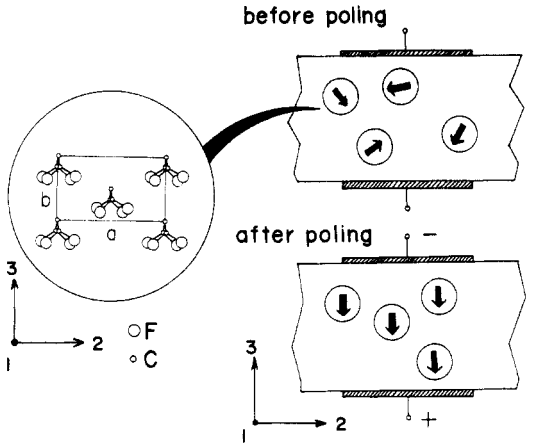

Figure 3. Illustration of structural change induced by the poling treatment of PVDF form I sample.

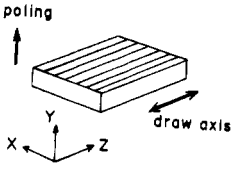

Figure 4. Definition of the coordinate system fixed on the sample film.

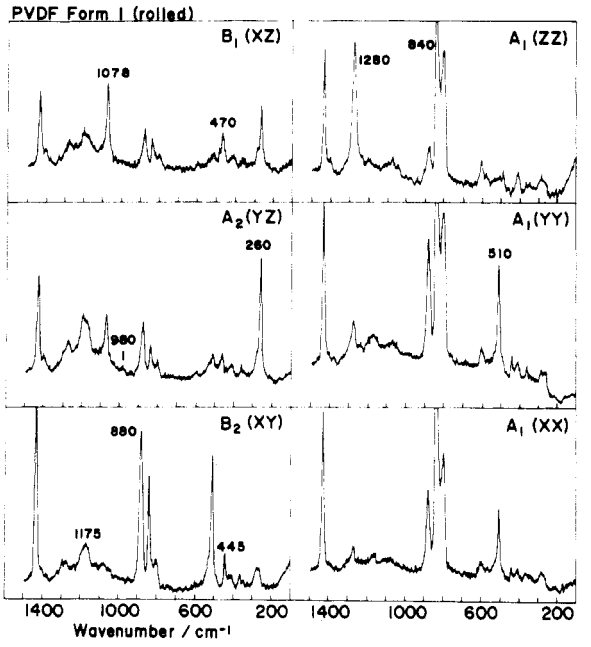

Figure 5. Polarized Raman spectra of rolled PVDF form I film (unpoled).

space-fixed coordinate axes are related to the crystal axes as $x \parallel b$, $y \parallel a$, and $z \parallel c$. That is to say, in the rolled PVDF form I sample, the polar b axis is considered to orient preferentially within the film plane or along the x axis. The samples obtained by cold-drawing the melt-quenched film at 60 °C are found to show a similar orientation character. These results are consistent with those of X-ray studies.[17]

In Figure 6 are reproduced a series of polarized Raman spectra taken with the (xz) and (yz) scattering geometries. Before poling the B_1 bands appear relatively strongly for the (xz) geometry and the A_2 bands appear for the (yz) geometry, as already pointed out above. But, when poling is carried out effectively (the efficiency could be checked by infrared measurement; refer to the caption of Figure 6), the (yz) component increases in relative intensity for the B_1 bands and the (xz) component increases for the A_2 bands, indicating that the orientation state of the sample transfers to the coordinate system of $x \parallel a$, $y \parallel b$, and $z \parallel c$. A detailed estimation of the degree of the b-axis orientation is now being carried out. Although the Raman spectra have been considered not to be sensitive to the b-axis orientational change in PVDF form I,[18] the experimental results of Figure 6 indicate a high sensitivity of the Raman method in detecting such an orientational change.

Raman polarization measurements on three-dimensionally oriented polymer samples have been found to be useful for interpreting the complicated vibrational spectra, as illustrated for doubly oriented *atactic* poly(vinyl alcohol).[19] In Figure 7 are shown all the Raman polarization components for a highly poled PVDF form I film. Including the infrared spectra of Figure 2, most of the Raman bands can be reasonably assigned to the previously reported symmetry species[12] on the basis of their polarization characters. In the previous paper,[12] however, we assigned the band at 880 cm^{-1} with the perpendicular infrared dichroism to the A_1 species and that at 840 cm^{-1} to the B_2 species. Polarization measurements of Figure 7 (and also Figure 2) indicate these assignments should be reversed: 880 cm^{-1} to the B_2 species and 840 cm^{-1} to the A_1 species. Therefore we have recalculated the normal-mode frequencies for an isolated single chain and carried out a least-squares fitting of the observed frequency data. The

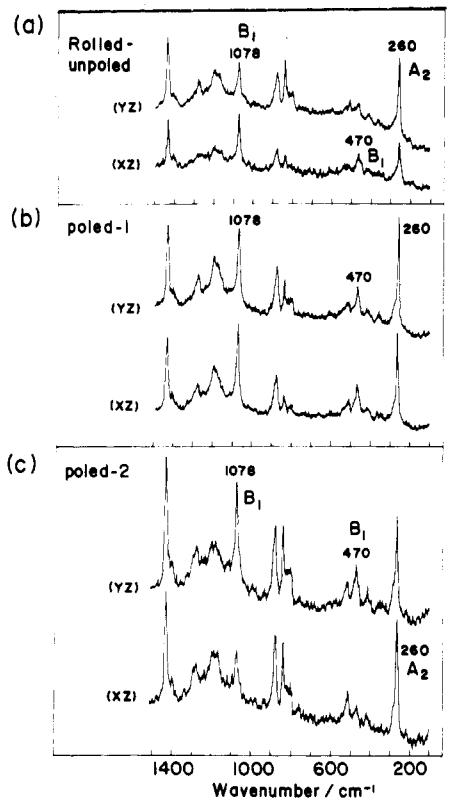

Figure 6. Polarized Raman spectra for the various PVDF form I films: (a) rolled and unpoled, (b) and (c) rolled and poled (corona poling at 10 kV, 30 min, room temperature, interelectrode distance 1 cm). The effectiveness of corona charging was not actually controlled because it was dependent largely on the condition of the sample films. We have checked qualitatively the poling efficiency by the relative intensity of $\nu_{as}(CH_2)$ and $\nu_s(CH_2)$ infrared bands (perpendicular component; refer to Figure 2). The ratio of absorbance $A(\nu_{as})/A(\nu_s)$ was about 1.1 for sample a, 1.5 for sample b, and 2.0 for sample c: the higher the ratio, the more effectively the sample is poled.

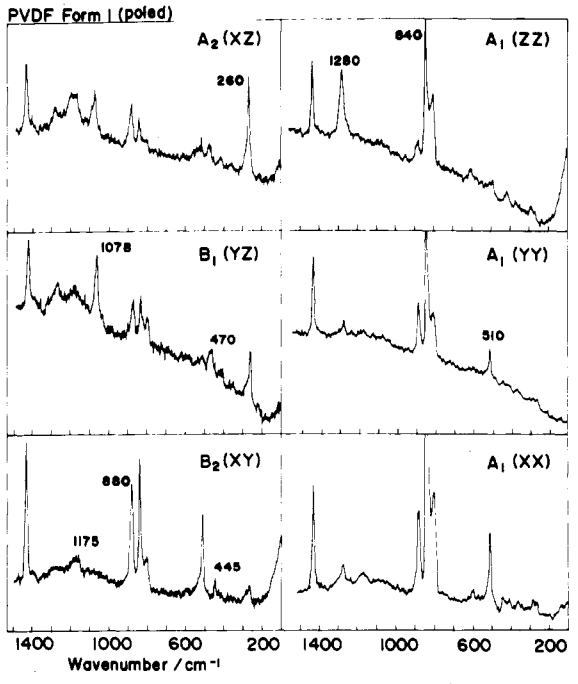

Figure 7. Polarized Raman spectra of highly poled PVDF form I film. The sample was the same as that used in Figure 2.

final results are listed in Table II. In Table III are shown the force constants obtained (valence force field).

Table II
Normal Coordinates Treatment of Single Chain of Poly(vinylidene fluoride) Form I

species	wavenumber, cm^{-1} obsd[a]	calcd[b]	PED (%)[c]
A_1	2980	2975	$\nu_s(CH_2)(99)$
	1428	1434	$\delta(CH_2)(81)$
	1273	1283	$\nu_s(CF_2)(40) - \nu_s(CC)(22) + \delta(CCC)(26)$
	840	844	$\nu_s(CF_2)(59) + \nu_s(CC)(17)$
	508	513	$\delta(CF_2)(98)$
A_2	980	980	$t(CH_2)(100)$
	260	265	$t(CF_2)(100)$
B_1	1398	1408	$w(CH_2)(58) - \nu_a(CC)(34)$
	1071	1074	$\nu_a(CC)(53) + w(CH_2)(25) - w(CF_2)(22)$
	468	471	$w(CF_2)(90)$
B_2	3022	3024	$\nu_a(CH_2)(99)$
	1177	1177	$\nu_a(CF_2)(71) - r(CF_2)(18)$
	880	883	$r(CH_2)(62) - \nu_a(CF_2)(18) - r(CF_2)(19)$
	442	444	$r(CF_2)(70) + r(CH_2)(24)$

[a] Infrared absorption spectral data (refer to Figure 2). [b] The utilized model was of planar-zigzag conformation. [c] Potential energy distribution. Symmetry coordinates: (ν_a) antisymmetric stretching; (ν_s) symmetric stretching; (δ) bending; (w) wagging; (t) twisting; (r) rocking. The sign + or − denotes the phase relation among the symmetry coordinates.

Table III
Intramolecular Valence Force Constants of Poly(vinylidene fluoride) Form I[a]

no.	coordinates involved	common atoms	values[b]
1	CH		4.901
2	CC		4.414
3	CC, CF	C	−0.091
4	CC, CC	C	0.148
5	CC, CCH	CC	0.206
6	CC, CCC	CC	0.273
7	CC, CCF	CC	0.548
8	CH, CH	C	0.058
9	CF		6.549
10	CF, CF	C	0.151
11	CF, CFF	CF	1.297
12	CCH		0.627
13	CCH, CCH	CC	0.105
14	CCH, CCH	CH	0.074
15	CHH		0.451
16	CCC		1.199
17	CCC, CCC (*t*)	CC	−0.036
18	CCF		1.387
19	CFF		1.506
20	CCCC		0.050
21	CF, CCF	CF	1.058
22	CCF, CCF	CC	0.176
23	CCF, CCF	CF	0.234
24	CCC, CCH (*g*)	CC	0.138
25	CCC, CCF (*g*)	CC	−0.083
26	CCH, CCF (*t*)	CC	0.063
27	CCH, CCF (*g*)	CC	0.055

[a] Refer to Table II in our previous paper.[12] [b] Units of force constants: stretch, mdyn/Å; bending, (mdyn Å)/rad^2; stretch-bending, mdyn/rad.

LO–TO Splitting in Raman Spectra of Poled PVDF Form I

On the basis of the factor group analysis of Table I, we can expect LO–TO splitting to occur for the polar symmetry species A_1, B_1, and B_2. The Raman measurement was carried out for a poled sample of PVDF form I in which the *b* axis orients preferably along the normal to the film plane. Raman spectral measurements were not easily made in the present study because of the following circumstances. (1) Highly three-dimensionally oriented film is needed to detect the LO–TO splitting, as explained below. Thus we had to utilize a thin film of 40-μm

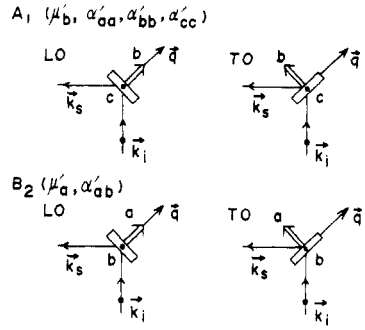

Figure 8. Scattering geometries for the measurement of the LO or TO bands illustrated for the A_1 and B_2 modes. In order to increase the intensity gain, we did not use the polarizer of the scattered Raman signals because the contribution of the band in question was considered to be overwhelmingly large for each scattering geometry, judging from the relative intensity of the bands shown in Figure 7.

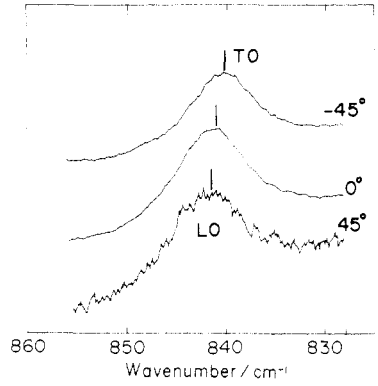

Figure 9. Frequency shift of the A_1 Raman band at 840 cm^{-1}. The angle is between the y axis of the sample and the incident photon vector $\boldsymbol{k}_i$. Refer to Figure 8.

thickness in order to increase the electric field strength so that the b-axis orientation is maximized as highly as possible. Such a thin film gave very weak Raman intensity, and the signal-to-noise ratio was not high. Although it might be possible to increase the S/N ratio of Raman bands by accumulating the data many times, we avoided the possibility of lowering the reproducibility of the frequency data by the repeated scanning process. In order to confirm the reproducibility of the band frequencies, we checked the frequency data by carrying out independent measurements an average of five times under the various spectral conditions. (2) The slight frequency shift of the Raman bands is difficult to detect because the bands are generally very broad in polymer systems, compared to low-molecular-weight single crystals. Although a sharpening of the bands was expected when the sample was cooled to liquid nitrogen temperature, no satisfactory spectral data of good S/N ratio could be obtained because of the great increase in fluorescence at low temperature.

In the Raman spectral measurements, 90° scattering geometry was employed. Therefore the phonon vector $\boldsymbol{q}$ points in the direction of +45° from the vertical line, as shown in Figure 8 ($\boldsymbol{q} = \boldsymbol{k}_i - \boldsymbol{k}_s$; $\boldsymbol{k}_i$ and $\boldsymbol{k}_s$ are wavevectors of incident and scattered laser beams). Measurements of the LO and TO bands of each symmetry species were carried out with the scattering geometries shown in Figure 8.

In Figures 9 and 10 are reproduced the Raman spectra of the A_1 bands at 840 and 1280 cm^{-1}, respectively. The A_1 vibrational bands have the transition dipole moment along the b axis. As seen in these figures, the peak position of the bands shifts by several wavenumbers in parallel with the change in the angle between the b axis and the phonon

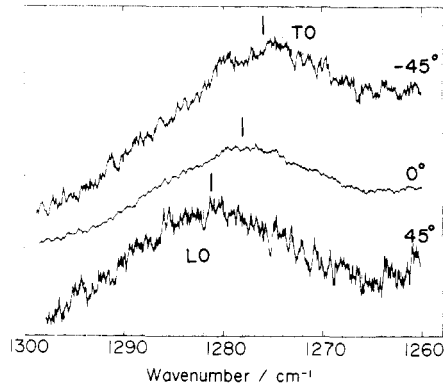

Figure 10. Frequency shift of the A_1 Raman band at 1280 cm^{-1}. The angle is between the y axis of the sample and the incident photon vector $\boldsymbol{k}_i$. Refer to Figure 8.

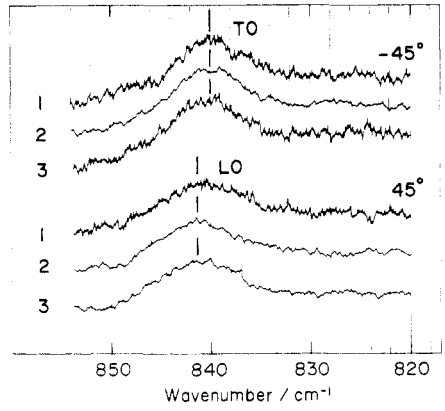

Figure 11. Raman spectra for the 840-cm^{-1} band taken with various spectral conditions in order to check the reproducibility of the band position. The angle is between the y axis of the sample and the incident photon vector $\boldsymbol{k}_i$.

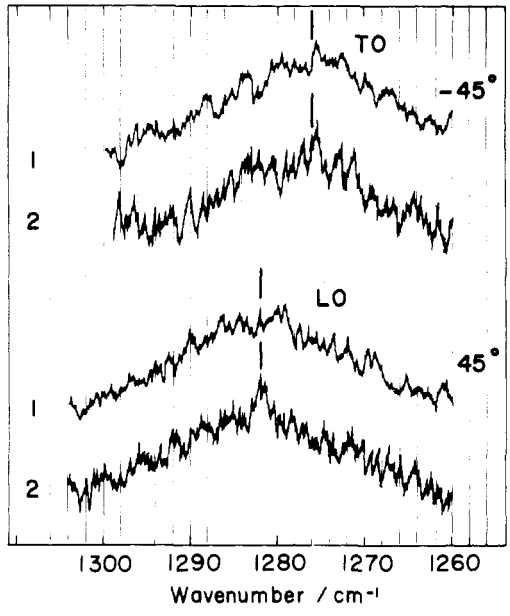

Figure 12. Raman spectra for the 1280-cm^{-1} band taken with various spectral conditions in order to check the reproducibility of the band position. The angle is between the y axis of the sample and the incident photon vector $\boldsymbol{k}_i$.

vector $\boldsymbol{q}$. The relation $\omega_{LO} > \omega_{TO}$, which should be required in general,[4-6] is also reasonable. In Figures 11 and 12 the reproducibility of the wavenumbers for the 840 and 1280 cm^{-1} bands is checked. These were taken by modifying measuring conditions such as scanning rate, response time of the recorder, and intensity and/or wavenumber

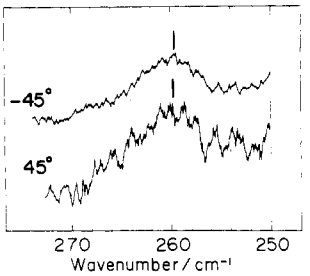

Figure 13. Raman spectra for the 260-cm^{-1} band (A_2 species). The angle is between the y axis of the sample and the incident photon vector $\boldsymbol{k}_i$. Refer to Figure 8.

Table IV
Observed LO and TO Frequencies for Poled Poly(vinylidene fluoride) Form I

species	ω_{LO}, cm^{-1}	ω_{TO}, cm^{-1}	IR, cm^{-1}	$\Delta\omega$, cm^{-1}
A_1	1282	1276	1273	6
	842	840	840	2
	509	508	508	1
B_2	881	880	880	1
A_2	260	260		0

scale in the recording sheet. For the nonpolar A_2 vibrational band at 260 cm^{-1}, no frequency shift was observed, as shown in Figure 13. The measured LO–TO splittings are listed in Table IV. The ω_{TO}'s are compared with the observed infrared frequencies because they should in principle be coincident with each other. The measurements for the other Raman bands were not successful in the present study because of their weak intensities and low S/N ratios.

Discussion

The observed LO–TO splitting is about 1–6 cm^{-1}, as seen in Table IV. In molecular crystals such as trioxane[7,8] and triglycine sulfate,[10] the LO–TO splitting is not as large as expected in ionic crystals. This may originate from the fact that in the potential field the short-range intermolecular forces are much greater than the long-range electrostatic forces. When the damping effect is neglected, the vibrational frequency ω of polar mode j is given by the sequential equation[6]

$$|(\omega_{TO}^2 - \omega^2)\delta_{jj'} + \frac{4\pi}{\epsilon^\infty(\hat{\boldsymbol{q}})}(\hat{\boldsymbol{q}}\cdot\boldsymbol{M}_j)(\hat{\boldsymbol{q}}\cdot\boldsymbol{M}_{j'})| = 0 \qquad (1)$$

where $\hat{\boldsymbol{q}}$ denotes the unit vector of phonon $\boldsymbol{q}$ and $\boldsymbol{M}_j$ is the transition moment of the jth mode. $\epsilon^\infty(\hat{\boldsymbol{q}}) = \sum_\alpha \epsilon^\infty{}_\alpha \hat{\boldsymbol{q}}^2{}_\alpha$ ($\alpha = x, y$, and z), and $\epsilon^\infty{}_\alpha$ is the dielectric constant at infinitely high frequency. Originally eq 1 includes a coupling term between the j and j' modes. But we can assume that in molecular crystals the mode–mode coupling is not so large, judging from the small LO–TO splitting. Under such an assumption, eq 1 becomes simplified as follows for the jth vibrational mode:

$$\omega_j^2 = \omega_{TOj}^2 + \frac{4\pi}{\epsilon^\infty(\hat{\boldsymbol{q}})}(\hat{\boldsymbol{q}}\cdot\boldsymbol{M}_j)^2 \qquad (2)$$

In the case of $M_j = 0$, i.e., for the nonpolar mode, ω_j is equal to ω_{TO} and not dependent on the angle between $\boldsymbol{q}$ and $\boldsymbol{M}_j$. In the case of $M_j \neq 0$, $\omega_j = \omega_{LO}$ corresponds to the case of $\boldsymbol{q} \parallel \boldsymbol{M}_j$. For $\boldsymbol{q} \perp \boldsymbol{M}_j$, ω_j is equal to ω_{TO}. In the orthorhombic system, only diagonal dielectric components ϵ_α^∞ are nonzero.[20] Therefore, for the principal axis of the crystal, ω_{LO} is given by

$$\omega_{LO}^2 = \omega_{TO}^2 + \frac{4\pi M_\alpha^2}{\epsilon_\alpha^\infty} \qquad (3)$$

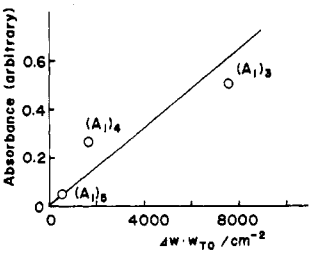

Figure 14. Plot of relative absorbance A (integrated value) against $\omega_{TO}\Delta\omega$ for the bands at 1280, 840, and 510 cm^{-1}.

Since the LO–TO splitting is quite small in the present case, eq 3 can be approximated as

$$\Delta\omega = \omega_{LO} - \omega_{TO} \doteq \frac{2\pi M_\alpha^2}{\epsilon_\alpha^\infty \omega_{TO}} \qquad (4)$$

This equation says that the LO–TO splitting $\Delta\omega$ is approximately proportional to M_α^2/ω_{TO}.[4-6] The infrared absorbance A_α is in proportion to the square of the transition moment M_α, and then, from eq 4

$$A_\alpha \propto \omega_{TO}\Delta\omega \qquad (5)$$

For PVDF form I, we evaluated the integrated intensity of the infrared absorbance for the bands at 1280, 840, and 510 cm^{-1}, where the sample used in the infrared spectral measurement was an unoriented film cast from hexamethylphosphoramide solution at room temperature and consisted of almost pure crystal form I.[12] As seen in Figure 14, a plot of the measured absorbance A against $\omega_{TO}\Delta\omega$ is, roughly speaking, consistent with eq 5.

The LO–TO splitting of Raman bands is observed also for vinylidene fluoride–trifluoroethylene copolymers,[21] which have attracted much attention because of their ferroelectric phase transition[22] and large piezoelectricity.[23] We are now trying to evaluate the LO–TO splitting theoretically from the viewpoint of lattice dynamics for these ferroelectric fluorine polymers.

Acknowledgment. We are grateful to Kureha Chemical Co., Ltd., for supplying the sample of poly(vinylidene fluoride). This work was partly supported by the Grant-in-Aid on Special Project Research for "Organic Thin Films for Information Conversion" from the Ministry of Education, Science, and Culture of Japan.

Registry No. PVDF (homopolymer), 24937-79-9.

References and Notes

(1) Special issue on ferroelectircity of PVDF. *Ferroelectrics* **1981**, *32*.
(2) Tashiro, K.; Takano, K.; Kobayashi, M.; Chatani, Y.; Tadokoro, H. *Polymer* **1983**, *24*, 199.
(3) Lines, M. E.; Glass, A. M. "Principles and Application of Ferroelectrics and Related Materials"; Oxford University Press: London, 1977.
(4) Born, M.; Huang, K. "Dynamical Theory of Crystal Lattices"; Clarendon Press: Oxford, 1954.
(5) Hayes, W.; Loudon, R. "Scattering of Light by Crystals"; Wiley: New York, 1978.
(6) Shapiro, S. M.; Axe, J. D. *Phys. Rev. B: Solid State* **1972**, *6*, 2420.
(7) Kobayashi, M. *J. Chem. Phys.* **1982**, *76*, 1187.
(8) Kobayashi, M.; Furumi, K. *J. Chem. Phys.* **1982**, *76*, 4725.
(9) Kobayashi, M., unpublished data.
(10) Kobayashi, M.; Tashiro, K.; Yagi, N. *J. Appl. Phys. Jpn.*, in press.
(11) Hasegawa, R.; Takahashi, Y.; Chatani, Y.; Tadokoro, H. *Polym. J. (Tokyo)* **1972**, *3*, 600.
(12) Kobayashi, M.; Tashiro, K.; Tadokoro, H. *Macromolecules* **1975**, *8*, 158.
(13) Kepler, R. G.; Anderson, R. A. *J. Appl. Phys.* **1978**, *49*, 1232.
(14) Takahasi, N.; Odajima, A. *Ferroelectrics* **1981**, *32*, 49.

(15) Naegele, D.; Yoon, D. Y. *Appl. Phys. Lett.* **1978**, *33*, 132.
(16) Douglass, D. C.; McBrierty, V. J.; Wang, T. T. *J. Chem. Phys.* **1982**, *77*, 5826. *Appl. Phys. Lett.* **1982**, *41*, 1051.
(17) Mizuno, T.; Nakamura, K.; Murayama, N.; Okuda, K. *Polym. Prepr. Jpn.* **1981**, *30*, 676.
(18) Cessac, G. L.; Curro, J. G. *J. Polym. Sci., Polym. Phys. Ed.* **1974**, *12*, 695.
(19) Tashiro, K.; Kobayashi, M.; Tadokoro, H. *Polym. Bull. (Berlin)* **1978**, *1*, 61.
(20) Nye, J. F. "Physical Properties of Crystals"; Oxford University Press: Oxford, 1957.
(21) Tashiro, K.; Kobayashi, M., unpublished data.
(22) Tashiro, K.; Takano, K.; Kobayashi, M.; Chatani, Y.; Tadokoro, H. *Ferroelectrics* **1984**, *57*, 297.
(23) Yagi, T.; Higashihata, Y.; Fukuyama, K.; Sako, J. *Ferroelectrics* **1984**, *57*, 327.

Fluorescence Anisotropy Decay Studies of Local Polymer Dynamics in the Melt. 2. Labeled Model Compounds of Variable Chain Length

Jean Louis Viovy,* Curtis W. Frank,† and Lucien Monnerie

Laboratoire de Physico-Chimie Structurale et Macromoleculaire (L.A. CNRS 278), ESPCI, 75231 Paris Cedex 05, France. *Received March 15, 1985*

ABSTRACT: The fluorescence anisotropy decay (FAD) of a series of 9,10-dialkylanthracenes, with alkyl substituents ranging from 6 to 16 CH_2 groups, embedded in a melt of unlabeled polybutadiene is investigated in the temperature range 210–350 K. The results are compared with different theoretical dynamic models relevant for flexible alkyl chains or for polymers by using the quantitative evaluation procedure applied to labeled polybutadiene in the previous paper of this series. The orientation autocorrelation function (OACF) presents a nonexponential character that increases progressively with the length of the alkyl tail. For tails with 14 carbon atoms and more, the OACF corresponds very accurately to the 1-D diffusion observed in long-chain labeled polymers. This result probes rather unambiguously the chain length necessary for the "polymer-like" 1-D diffusion behavior to settle. Also, the evolution of the correlation times with the temperature and with the size of the molecule supports the idea, developed recently by Helfand and co-workers, that this 1-D diffusion corresponds to correlated conformational jumps.

I. Introduction

In the previous paper of this series, we presented fluorescence anisotropy decay (FAD) experiments performed at LURE-ACO, Orsay, France. Using synchrotron radiation as an exciting source, we recorded the orientation autocorrelation function (OACF) of a labeled polybutadiene chain embedded in a matrix of similar unlabeled polybutadiene in the time window 0.1–70 ns and in the temperature range 223–353 K. The experimental results have been compared with various models for main-chain polymer motions proposed in the literature.[2-7]

The shape of the OACF, which remains almost homothetic when the temperature is varied, is very similar to the one observed in dilute solutions.[7] Recent single-chain models of the dynamics, such as the Hall–Helfand[6] or generalized diffusion and loss[7] models, fit the data correctly at the present experimental precision. From these observations, we concluded that the major origin of the nonexponential character of the single-bond OACF is the connectivity of the chain. In comparison with dynamics in dilute solution, the surrounding chains affect segmental motions by means of an increase in the friction coefficient, but they do not seem to modify seriously their specific dynamic behavior.

We also observed that the orientation relaxation of the label follows the same temperature law as macroscopic properties (i.e., WLF equation[8,9]). Such a result implies that the local chain motions observed by FAD in polybutadiene are involved in the glass transition phenomenon. If one considers the experimental time scale (0.1–70 ns), the size of the label, and the amplitude of orientation relaxation required to affect the OACF, it is reasonable to assume that these chain motions correspond to conformation changes. However, it would be interesting to investigate their scale more quantitatively.

In the present paper, we present synchrotron-excited FAD experiments performed on a series of flexible fluorescent probes (9,10-dialkylanthracene) embedded in a matrix of nonfluorescent polybutadiene. By studying the evolution of the OACF as a function of the length of the alkyl tail, we aimed at further information about the molecular origin of the observed orientation relaxation. For instance, if, as we suspected, the nonexponential character of the OACF is mainly due to chain connectivity, it should increase with substituent length, and the rate of this increase should give direct information on the scale of the motions involved. We were also interested in the coupling between the flexible probes and the polymer matrix and in a comparison between the behavior of the probe and that of labeled long-chain polybutadiene.

In section II, the preparation of the samples and the experimental technique are briefly reviewed (for a more complete description please refer to part 1 of the series).[1] The experimental correlation functions and some general results are presented in section III. In sections IV and V, we compare quantitatively these results with relevant theoretical models, namely the Jones and Stockmayer[4] model, which considers flexible chains starting from the "short molecule" side, and the Hall and Helfand[6] and generalized diffusion and loss[7] models, which start from an "infinite chain" representation. Temperature effects are discussed in section VI, and the general molecular conclusions which can be drawn from the present study are summarized in section VII.

† Permanent address: Department of Chemical Engineering, Stanford University, Stanford, CA 94305.

0024-9297/85/2218-2606$01.50/0